Supporting Information for

Catechol oxidase activity of comparable dimanganese and dicopper complexes

Adriana M. Magherusan, Daniel N. Nelis, Brendan Twamley, Aidan R. McDonald*

School of Chemistry, Trinity College Dublin, The University of Dublin, College Green, Dublin 2, Ireland

E-mail: aidan.mcdonald@tcd.ie

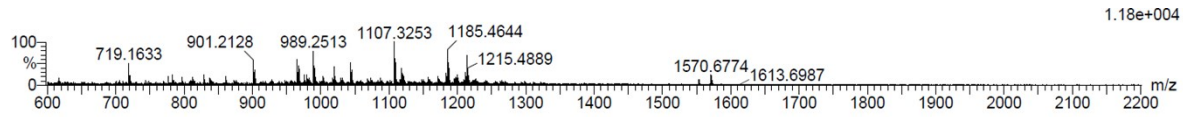

Minimum:				-1.5							
Maximum:		5.0	10.0	200.0							
Mass	Calc. Mass	mDa	PPM	DBE	i-FIT	i-FIT (Norm)	Formula				
989.2513	989.2470	4.3	4.3	24.5	55.4	0.0	C45	H52	N10	O7	Cl Mn2

Figure S1. Maldi-ToF mass spectrometry showing formation of complex **1**.

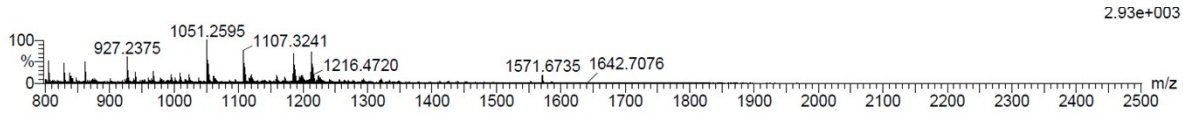

Minimum:				-1.5							
Maximum:		5.0	5.0	500.0							
Mass	Calc. Mass	mDa	PPM	DBE	i-FIT	i-FIT (Norm)	Formula				
1051.2595	1051.2626	-3.1	-2.9	28.5	50.3	0.0	C50	H54	N10	O7	Cl Mn2

Figure S2. Maldi-ToF mass spectrometry showing formation of complex **2**.

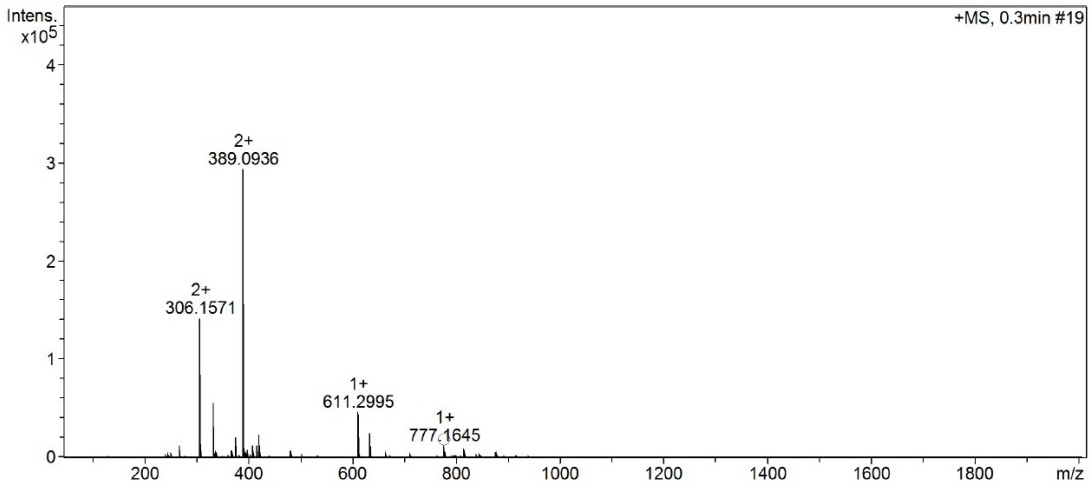

Meas. m/z	#	Ion Formula	m/z	err [mDa]	err [ppm]	rdb	N-Rule	e⁻ Conf	mSigma
777.164474	1	C37H35Mn2N10O3	777.164902	-0.4	-0.5	25.5	ok	even	44.1

Figure S3. ESI-MS showing formation of complex **3**.

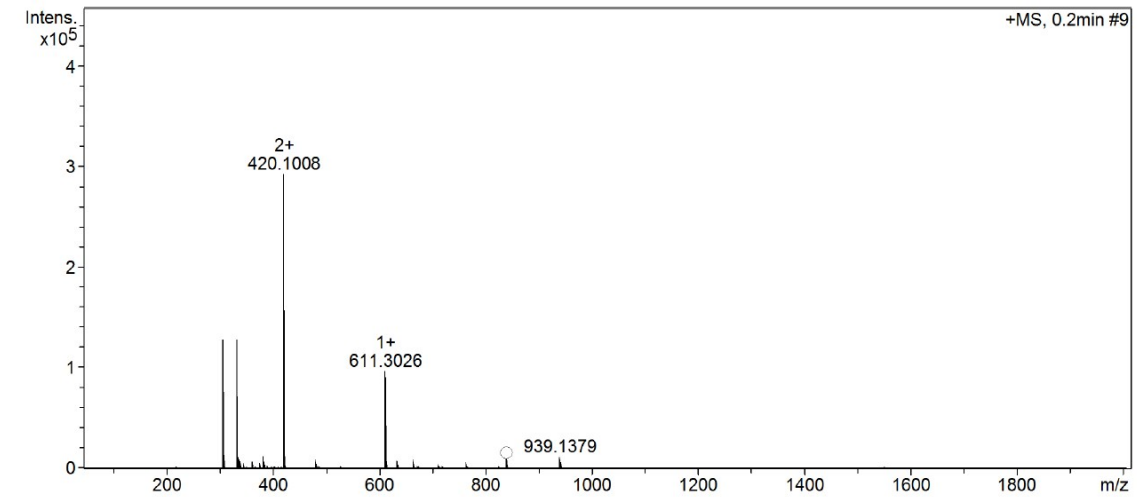

Meas. m/z	#	Ion Formula	m/z	err [mDa]	err [ppm]	rdb	N-Rule	e⁻ Conf	mSigma
839.179958	1	C42H37Mn2N10O3	839.180552	-0.6	-0.7	29.5	ok	even	13.5

Figure S4. ESI-MS showing formation of complex **4**.

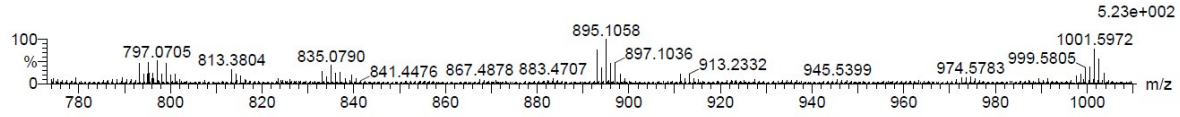

Minimum:				-1.5			
Maximum:		5.0	20.0	500.0			
Mass	Calc. Mass	mDa	PPM	DBE	i-FIT	i-FIT (Norm)	Formula
893.1071	893.1049	2.2	2.5	24.5	73.1	0.0	C37 H36 N10 O7 Cl Cu2

Figure S5. ESI-MS showing formation of complex **5**.

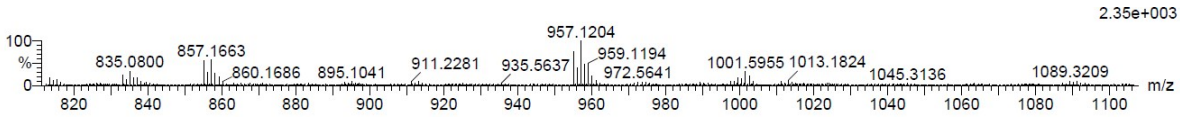

Minimum:				-1.5			
Maximum:		5.0	20.0	500.0			
Mass	Calc. Mass	mDa	PPM	DBE	i-FIT	i-FIT (Norm)	Formula
955.1213	955.1205	0.8	0.8	28.5	79.5	0.0	C42 H38 N10 O7 Cl Cu2

Figure S6. ESI-MS showing formation of complex **6**.

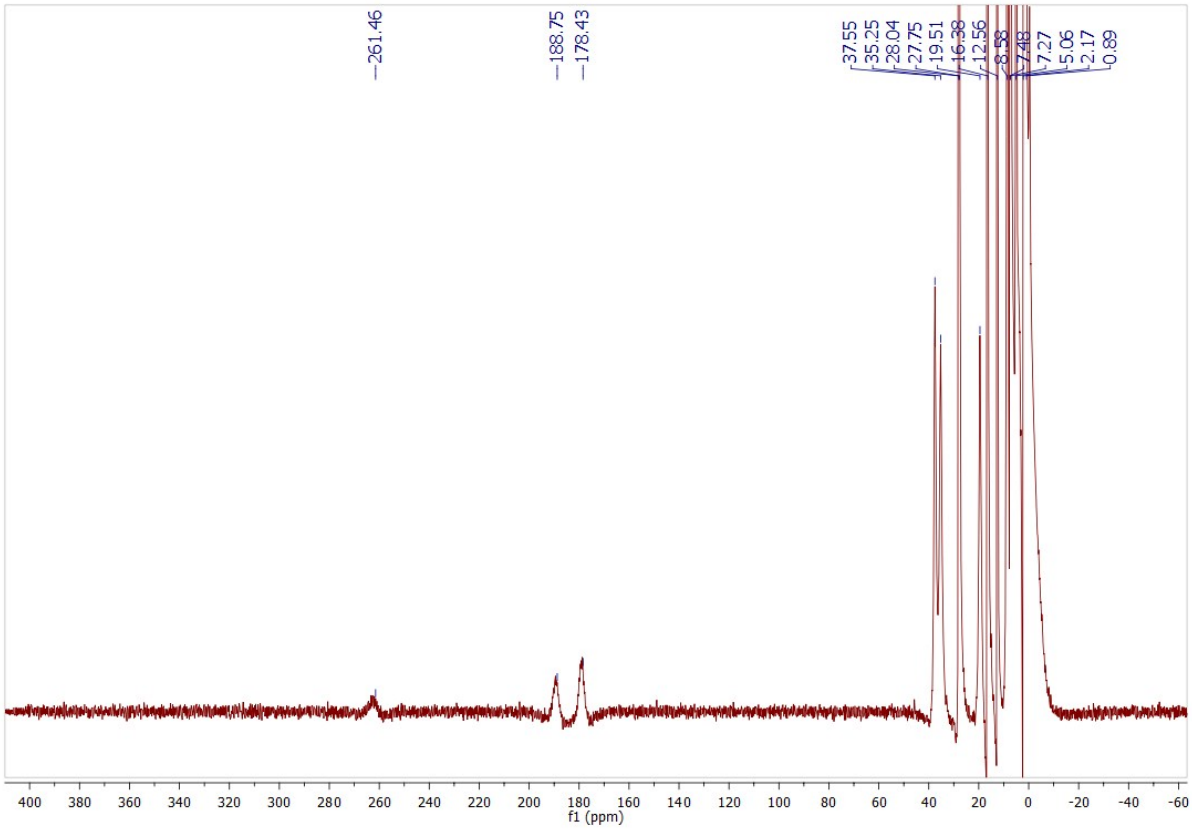

Figure S7. ^{1}H NMR of complex **5** in CD_3CN.

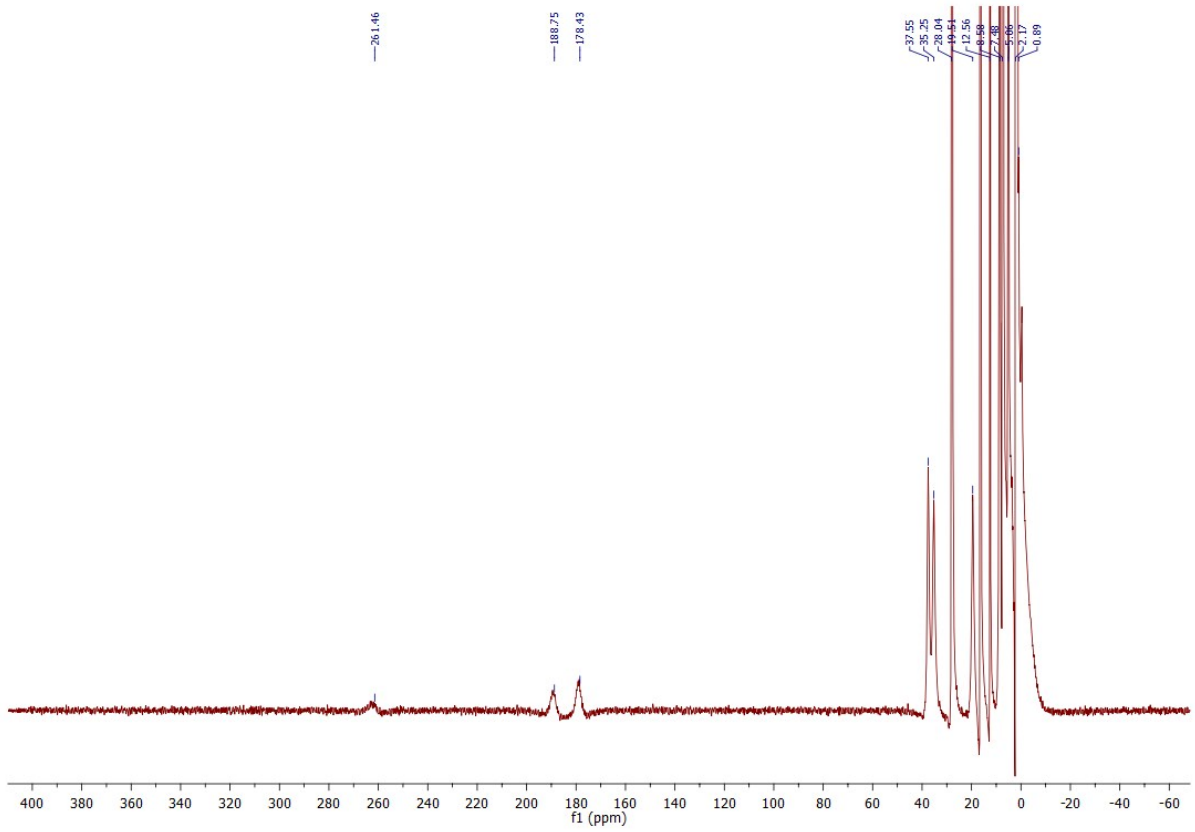

Figure S8. ^{1}H NMR of complex **6** in CD_3CN.

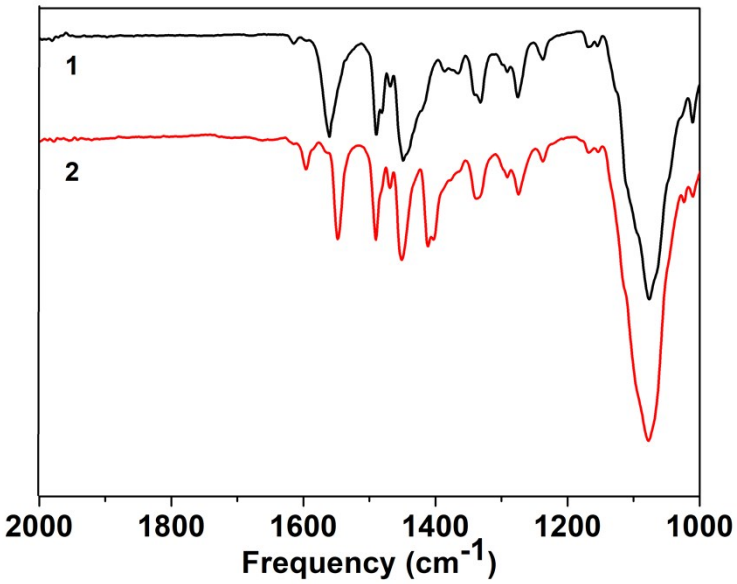

Figure S9. ATR-FTIR spectra of manganese complexes **1** (black) and **2** (red).

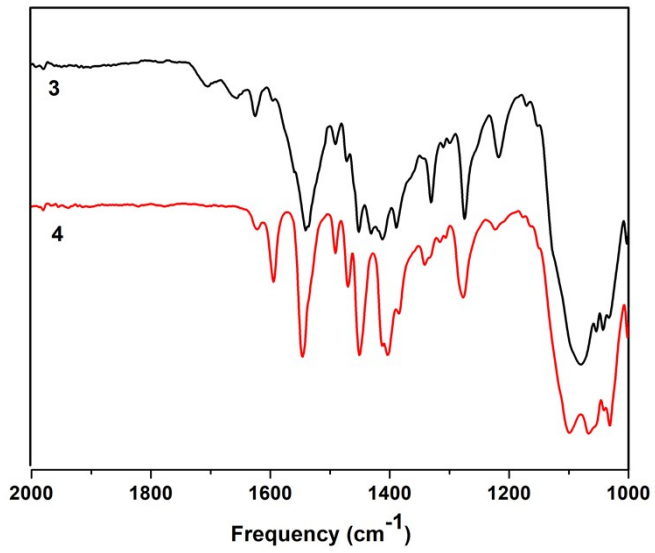

Figure S10. ATR-FTIR spectra of manganese complexes **3** (black) and **4** (red).

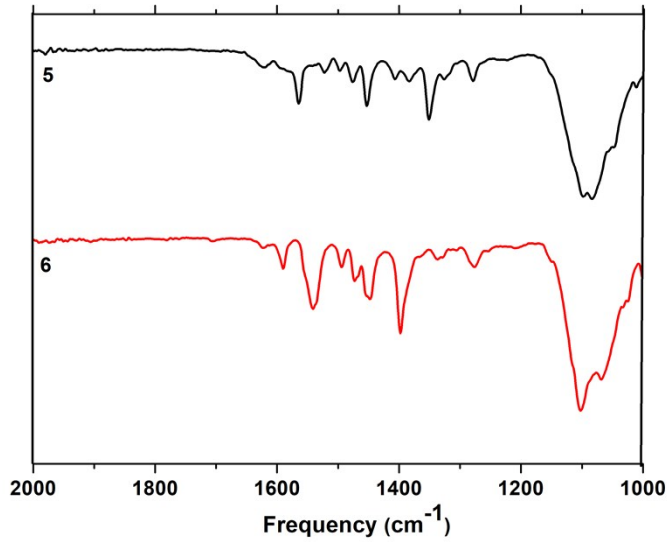

Figure S11. ATR-FTIR spectra of copper complexes **5** (black) and **6** (red).

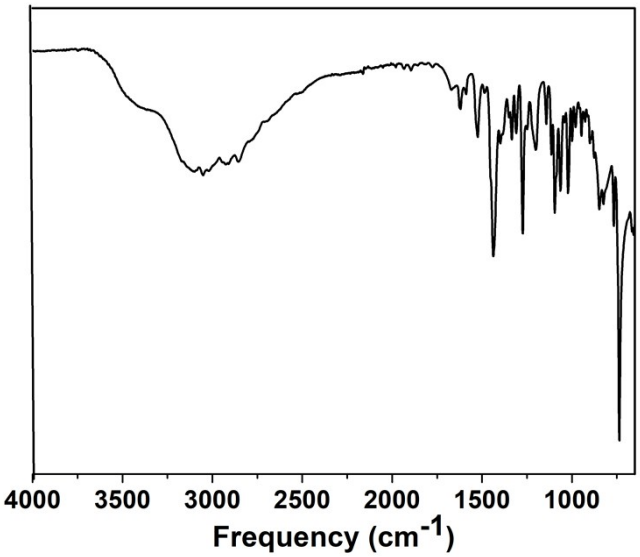

Figure S12. ATR-FTIR spectrum of HPTB ligand.

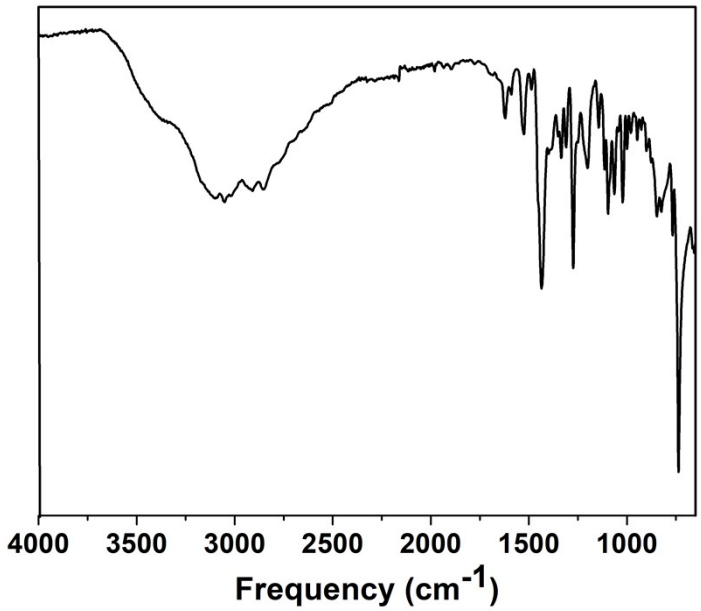

Figure S13. ATR-FTIR of N-Et-HPTB ligan.

Complexes		**1**[1]	**2**	**3**[2]	**4**	**5**	**6**
Average Bond Lengths (M = metal)	M-N_{amine} (Å)	2.42	2.39	2.45	2.43	2.13	2.12
	M-N_{benz} (Å)	2.13	2.13	2.18	2.13	2.08	2.08

Table S1. Comparison of average bond lengths in complexes **1**-**6**.

X-Ray Diffraction Methods and Structure Refinements

Complex 2. A specimen of $C_{56}H_{63}Cl_2Mn_2N_{13}O_{11}$, approximate dimensions 0.050 mm x 0.075 mm x 0.080 mm, was used for the X-ray crystallographic analysis using a MiTeGen micromount. Bruker APEX software was used to collect, correct for Lorentz and polarization effects and reduce the data.[3] One perchlorate molecule was disordered. This disorder was modelled with constraints and restraints (DFIX, EADP) yielding a three-positional model with occupancies of 0.38217, 0.39796 and 0.21986.

Complex 4. A specimen of $C_{46}H_{43}Cl_2Mn_2N_{12}O_{11}$, approximate dimensions 0.090 mm x 0.110 mm x 0.180 mm, was used for the X-ray crystallographic analysis using a MiTeGen micromount. Bruker APEX software was used to correct for Lorentz and polarization effects. [3] Three benzimidazoles modelled as disordered as well as two linking carbons C20, C36 and the bridge carbons C22 and C25. These were modelled with 80:20% occupancy with restraints (DFIX, SADI, FLAT) and constraints (EADP, AFIX 66). Both perchlorates were also modelled in two positions with 58% and 67% major occupancy. Constraints (EADP, rigid model) used. The molecule was refined as a racemic twin with a refined twin ratio of 0.49(5).

Complex 5. A specimen of $C_{42}H_{41.50}Cl_2Cu_2N_{11.50}O_{11.50}$, approximate dimensions 0.070 mm x 0.110 mm x 0.340 mm, was used for the X-ray crystallographic analysis using a MiTeGen micromount. Bruker APEX software was used to correct for Lorentz and polarization effects. [3] There were 4 partially occupied MeCN molecules in asymmetric unit. N51, 43; N54, 62; N59, 31; N62, 14% occupied. Total = 1.5 MeCN per asymmetric unit. One perchlorate Cl1/Cl3 is disordered over two positions with occupancies of 54:46%. Cl3 perchlorate shares space with a half-occupied diethyl ether molecule. Restraints (DFIX, SADI, ISOR, SUMP for MeCN occupancy) and constraints (EADP) were used in the model.

Complex 6. A specimen of $C_{45}H_{42.50}Cl_2Cu_2N_{11.50}O_{11}$, approximate dimensions 0.140 mm x 0.190 mm x 0.370 mm, was used for the X-ray crystallographic analysis using a MiTeGen micromount. Bruker APEX software was used to collect, correct for Lorentz and polarization effects and reduce the data.[3] One perchlorate was modelled in two positions with a refined occupancy of 54:46% with one shared oxygen atom O68. Constraints were used to model this disorder (EADP). Restraints were used in the model of the free solvent MeCN groups (SADI, ISOR) one of which is only half occupied.

Table S2. Crystal data and structure refinement for complexes **2**, **4**-**6**.

	(**2**)	(**4**)	(**5**)	(**6**)
Name:	$[Mn_2(O_2CPh)(N\text{-}Et\text{-}HPTB)](ClO_4)_2$	$[Mn_2(O_2CPh)(HPTB)](ClO_4)_2$	$[Cu_2(O_2CCH_3)(HPTB)](ClO_4)_2$	$[Cu_2(O_2CPh)(HPTB)](ClO_4)_2$
Empirical formula	$C_{56}H_{63}Cl_2Mn_2N_{13}O_{11}$	$C_{46}H_{43}Cl_2Mn_2N_{12}O_{11}$	$C_{42}H_{45.50}Cl_2Cu_2N_{11.50}O_{11.50}$	$C_{45}H_{42.50}Cl_2Cu_2N_{11.50}O_{11}$
Formula weight	1274.97	1120.70	1093.38	1118.38
Temperature (K)	100(2)	100(2)	100(2)	100(2)
Wavelength (Å)	1.54178	0.71073	0.71073	0.71073
Crystal system	Triclinic	Monoclinic	Triclinic	Monoclinic
Space group	$P\bar{1}$	Cc	$P\bar{1}$	Cc
a (Å)	13.0800(4)	21.3934(11)	12.8864(8)	20.4647(8)
b (Å)	14.4180(5)	21.7926(11)	13.1530(8)	21.8424(8)
c (Å)	17.9989(5)	11.6260(6)	16.6060(11)	11.5893(4)
α (°)	73.3874(19)	90	80.111(2)	90
β (°)	78.3545(18)	115.314(3)	71.250(2)	111.2580(10)
γ (°)	66.9439(18)	90	61.8690(10)	90
Volume ($Å^3$)	2977.27(17)	4899.8(4)	2349.7(3)	4827.9(3)
Z	2	4	2	4
Density (calc, Mg/m^3)	1.422	1.519	1.545	1.539
ρ (mm^{-1})	4.860	0.698	1.092	1.064
F(000)	1324	2300	1124	2292
Crystal size (mm^3)	0.080 x 0.075 x 0.050	0.18 x 0.11 x 0.09	0.34 x 0.11 x 0.07	0.37 x 0.19 x 0.14
Index ranges	-15≤h≤15, -17≤k≤17, -21≤l≤21	-26≤h≤26, -26≤k≤26, -14≤l≤14	-16≤h≤16, -16≤k≤16, -20≤l≤20	-25≤h≤25, -27≤k≤27, -14≤l≤14
Reflections collected	56368	68365	55045	41111
Independent reflections	10484 [R(int) = 0.0970]	9586 [R(int) = 0.0788]	9654 [R(int) = 0.0227]	10007 [R(int) = 0.0394]
Absorption correction	Numerical	Semi-empirical from equivalents	Semi-empirical from equivalents	Semi-empirical from equivalents
Max. and min. transmission	0.9694 and 0.7652	0.7455 and 0.6867	0.7454 and 0.6674	0.7454 and 0.7002
Data / restraints / parameters	10484 / 31 / 787	9586 / 27 / 544	9654 / 35 / 690	10007 / 34 / 656
Goodness-of-fit on F^2	1.038	1.120	1.042	1.059
R indices [I>2σ(I)]	R1 = 0.0593, wR2 = 0.1470	R1 = 0.0766, wR2 = 0.1598	R1 = 0.0658, wR2 = 0.1727	R1 = 0.0427, wR2 = 0.1082
R indices (all data)	R1 = 0.0876, wR2 = 0.1665	R1 = 0.0977, wR2 = 0.1703	R1 = 0.0713, wR2 = 0.1770	R1 = 0.0487, wR2 = 0.1123
Flack Parameter	-	0.49(5)	-	0.276(15)
Largest diff. peak and hole ($e.Å^{-3}$)	0.531 and -0.702	0.722 and -0.642	2.020 and -2.020	0.866 and -0.724
CCDC no.	1476678	1822648	1822647	1822646

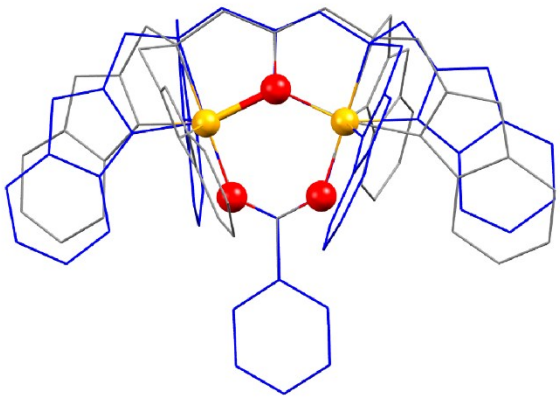

Figure S14. Overlapping structure of Cu^{II}_2 complexes **5** (grey wireframe) and **6** (blue wireframe)**.**

Cyclic Voltammograms of Complexes 1-6

The oxidation potentials for complexes **1-4** and reduction potentials for complexes **5-6** were measured by CV using a glassy carbon working electrode in acetonitrile solution containing 0.1 M NBu_4PF_6 as the supporting electrolyte. The counter electrode used was platinum while the reference electrode was $AgNO_3$.

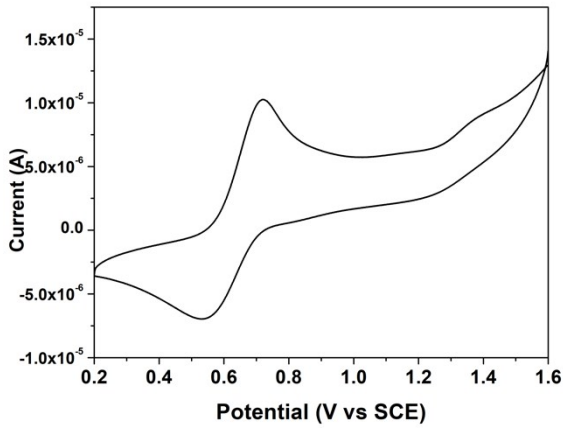

Figure S15. Cyclic voltammogram of complex **1** (1 mM) in acetonitrile containing NBu_4PF_6 (0.1 M) as supporting electrolyte at 100 mV/s. The initial scan voltammogram of the first cycle was done from negative to positive (initial potential 0.2 V vs SCE).

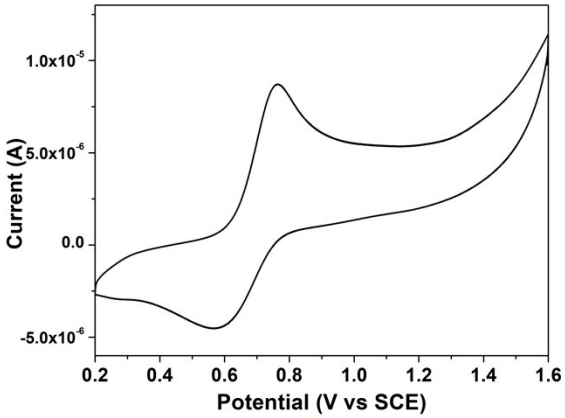

Figure S16. Cyclic voltammogram of complex **2** (1 mM) in acetonitrile containing NBu_4PF_6 (0.1 M) as supporting electrolyte at 100 mV/s. The initial scan voltammogram of the first cycle was done from negative to positive (initial potential 0.2 V vs SCE).

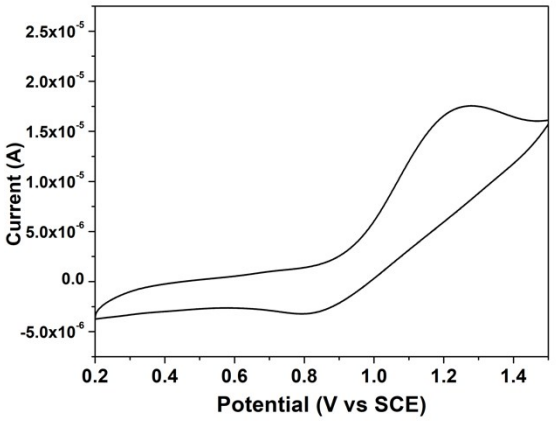

Figure S17. Cyclic voltammogram of complex **3** (1 mM) in acetonitrile containing NBu_4PF_6 (0.1 M) as supporting electrolyte at 100 mV/s. The initial scan voltammogram of the first cycle was done from negative to positive (initial potential 0.2 V vs SCE).

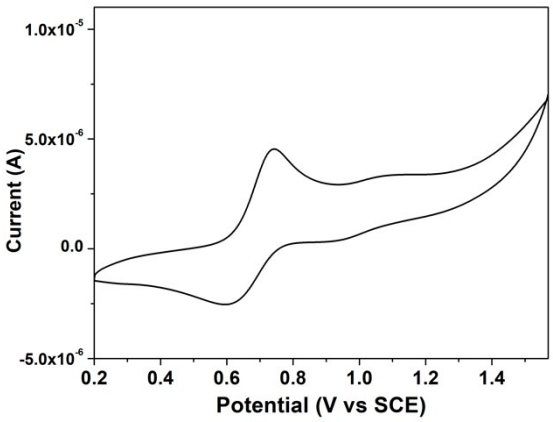

Figure S18. Cyclic voltammogram of complex **4** (1 mM) in acetonitrile containing NBu_4PF_6 (0.1 M) as supporting electrolyte at 50 mV/s. The initial scan voltammogram of the first cycle was done from negative to positive (initial potential 0.2 V vs SCE).

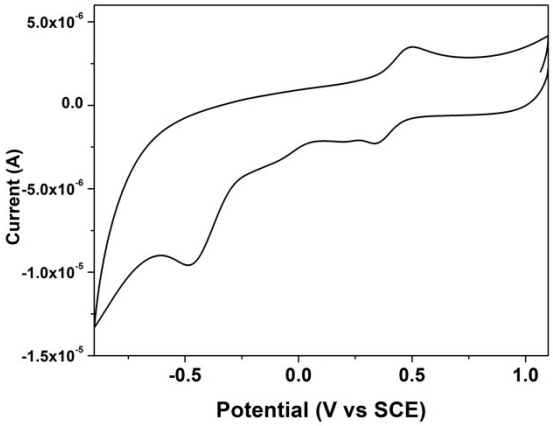

Figure S19. Cyclic voltammogram of complex **5** (1 mM) in acetonitrile containing NBu_4PF_6 (0.1 M) as supporting electrolyte at 50 mV/s. The initial scan voltammogram of the first cycle was done from negative to positive (initial potential 0.2 V vs SCE).

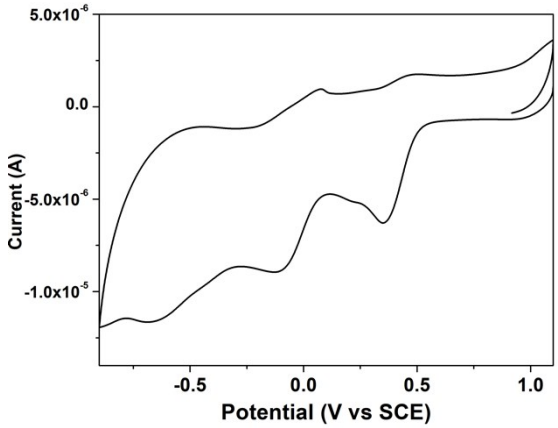

Figure S20. Cyclic voltammogram of complex **6** (1 mM) in acetonitrile containing NBu_4PF_6 (0.1 M) as supporting electrolyte at 50 mV/s. The initial scan voltammogram of the first cycle was done from negative to positive (initial potential 0.2 V vs SCE).

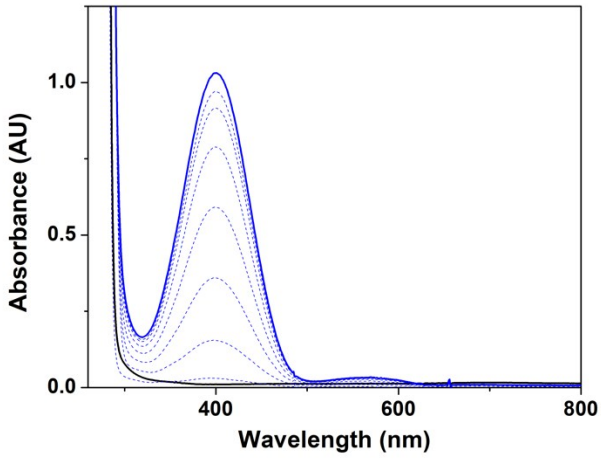

Figure S21. Electronic absorption spectral changes showing formation of 3,5-DTBQ (blue trace) after addition of 3,5-DTBC (25 equivalents, 50 µl) to complex **1** (0.1 mM, black trace) in acetonitrile at 25 °C.

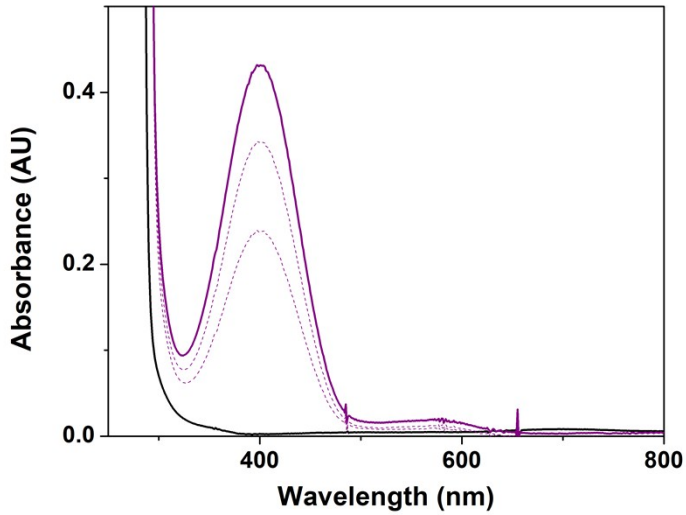

Figure S22. Electronic absorption spectral changes showing formation of 3,5-DTBQ (purple trace) after addition of 3,5-DTBC (25 equivalents, 50 µl) to complex **3** (0.1 mM, black trace) in acetonitrile at 25 °C.

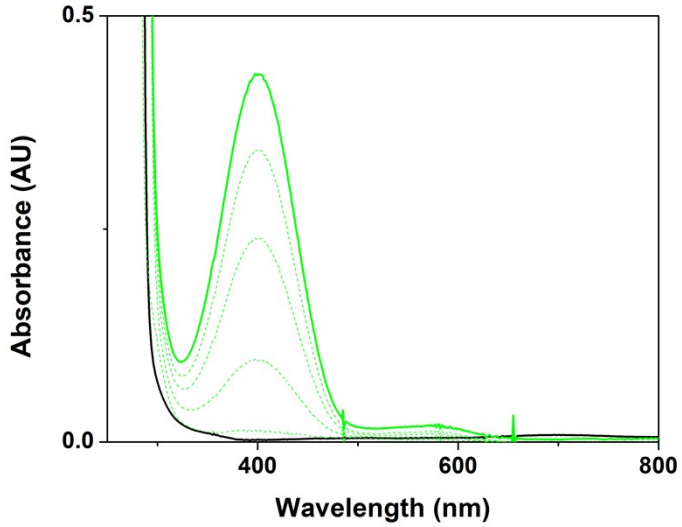

Figure S23. Electronic absorption spectral changes showing formation of 3,5-DTBQ (green trace) after addition of 3,5-DTBC (25 equivalents, 50 µl) to complex **4** (0.1 mM, black trace) in acetonitrile at 25 °C.

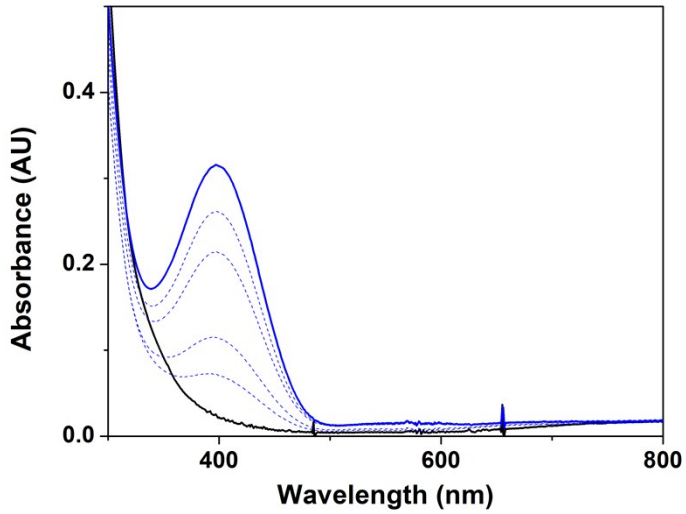

Figure S24. Electronic absorption spectral changes showing formation of 3,5-DTBQ (blue trace) after addition of 3,5-DTBC (25 equivalents, 50 µl) to complex **5** (0.1 mM, black trace) in acetonitrile at 25 °C.

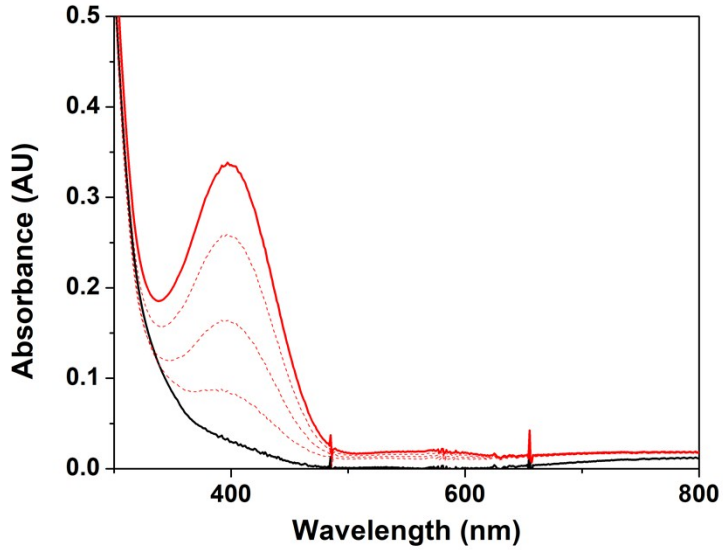

Figure S25. Electronic absorption spectral changes showing formation of 3,5-DTBQ (red trace) after addition of 3,5-DTBC (25 equivalents, 50 µl) to complex **6** (0.1 mM, black trace) in acetonitrile at 25 °C.

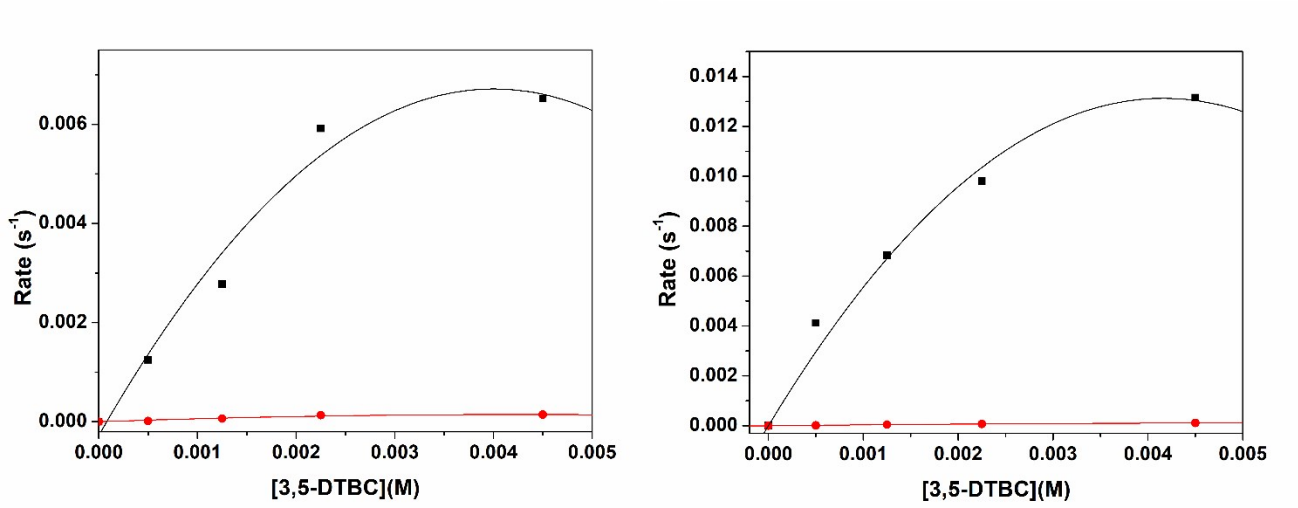

Figure S26. Dependence of the first order reaction rate of the first (black trace) and second phases (red trace) on 3,5-DTBC concentrations for complexes **5** (left) and **6** (right).

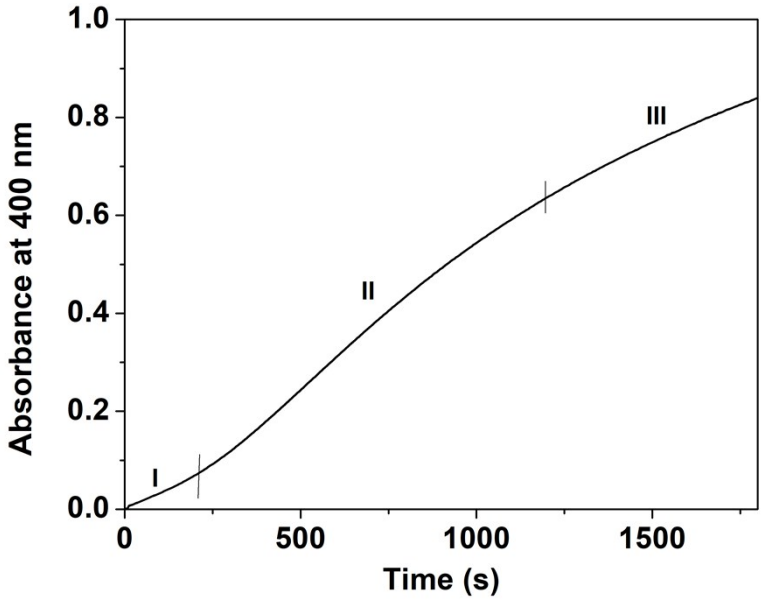

Figure S27. Plot of absorbance at 400 nm versus time for Mn^{II}_2 complex **1**.

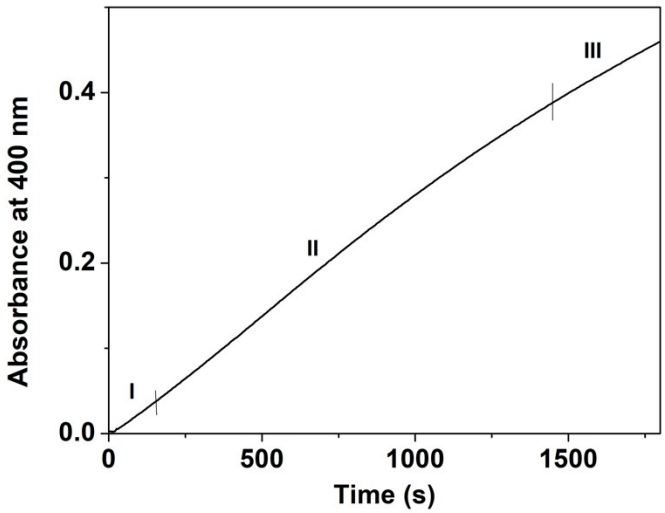

Figure S28. Plot of absorbance at 400 nm versus time for Mn^{II}_2 complex **2**.

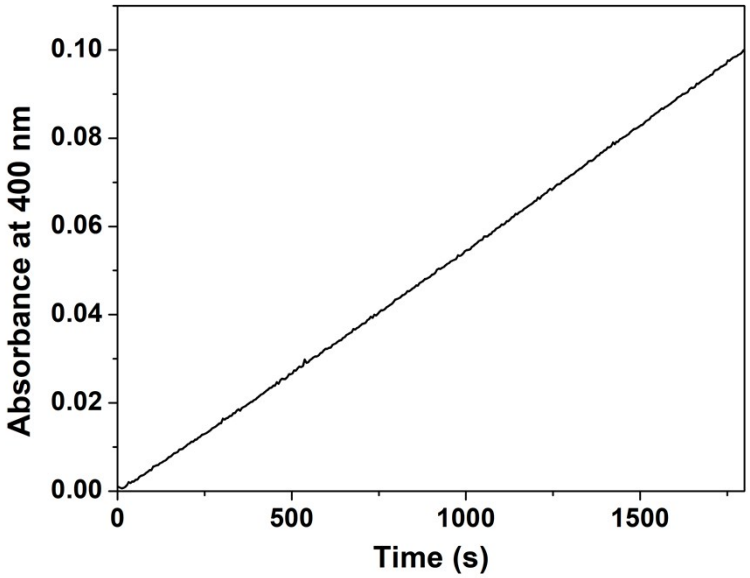

Figure S29. Plot of absorbance at 400 nm versus time for Mn^{II}_2 complex **3**.

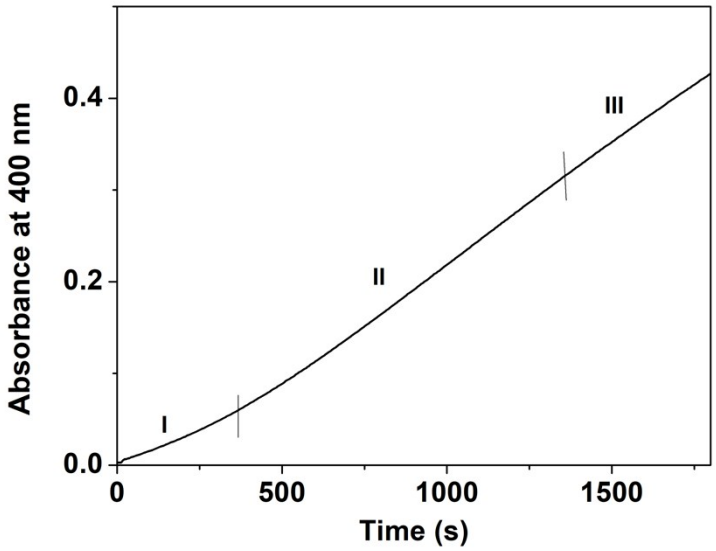

Figure S30. Plot of absorbance at 400 nm versus time for Mn^{II}_2 complex **4**.

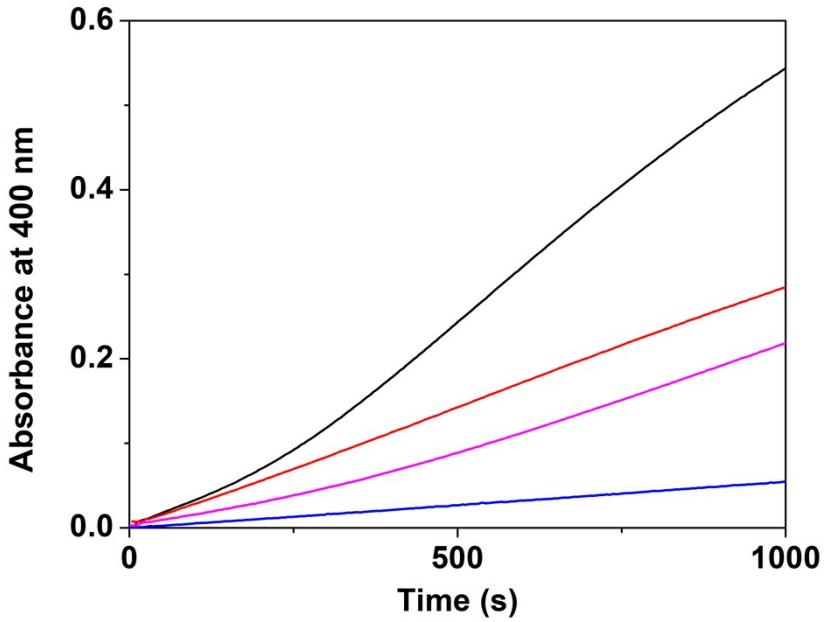

Figure S31. Expansion of Figure 7, plot of absorbance at λ_{max} = 400 nm versus time for the reaction between Mn^{II}_2 complexes **1** (black trace), **2** (red trace), **3** (blue trace), and **4** (pink trace) and 25 equivalents 3,5-DTBC in acetonitrile.

Complex **1**		Complex **2**		Complex **4**	
[3,5-DTBC] (M)	**Rate constant (s^{-1})**	**[3,5-DTBC] (M)**	**Rate constant (s^{-1})**	**[3,5-DTBC] (M)**	**Rate constant (s^{-1})**
$2.5*10^{-4}$		$5*10^{-4}$		$5*10^{-4}$	
1st phase	$1.9*10^{-3}$	First phase	$2.65*10^{-3}$	First phase	$6.13*10^{-3}$
Second phase	$4*10^{-4}$	Second phase	$1.33*10^{-4}$	Second phase	$2.4*10^{-4}$
Third phase	$3.5*10^{-4}$	Third phase	$5.4*10^{-4}$	Third phase	$4.6*10^{-4}$
$5*10^{-4}$		$8*10^{-4}$		$8*10^{-4}$	
First phase	$2.05*10^{-3}$	First phase	$2.1*10^{-3}$	First phase	$6.27*10^{-3}$
Second phase	$6.2*10^{-4}$	Second phase	$2.25*10^{-4}$	Second phase	$2.8*10^{-4}$
Third phase	$3.6*10^{-4}$	Third phase	$5.1*10^{-4}$	Third phase	$4.8*10^{-4}$
$8*10^{-4}$		$1.25*10^{-3}$		$1.25*10^{-3}$	
First phase	$2.5*10^{-3}$	First phase	$2.2*10^{-4}$	First phase	$5.9*10^{-3}$
Second phase	$7.4*10^{-4}$	Second phase	$2.8*10^{-4}$	Second phase	$3.6*10^{-4}$
Third phase	$3.9*10^{-4}$	Third phase	$4.8*10^{-4}$	Third phase	$3.11*10^{-4}$
		$2.25*10^{-3}$		$2.25*10^{-3}$	
		First phase	$2.6*10^{-3}$	First phase	$5.8*10^{-3}$
		Second phase	$3.35*10^{-4}$	Second phase	$4.1*10^{-4}$
		Third phase	$3.6*10^{-4}$	Third phase	$2.8*10^{-4}$

Table S3. Approximate (**estimated**) rate constant values of the three phases of reaction for Mn^{II}_2 complexes **1**, **2** and **4**.

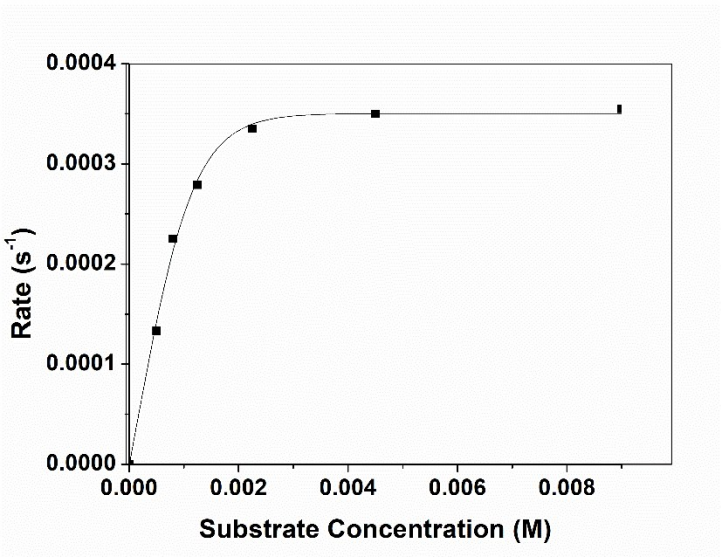

Figure S32. Plot of first order approximate reaction rates of the second phase of the reaction of complex **2** (0.1 mM) against 3,5-DTBC concentrations. All measurements were carried out in acetonitrile at 25 °C.

References

1. A. M. Magherusan, A. Zhou, E. R. Farquhar, M. Garcia-Melchor, B. Twamley, L. Que, Jr. and A. R. McDonald, *Angew. Chem. Int. Ed. Engl.*, 2018, **57**, 918-922.
2. P. J. Pessiki, S. V. Khangulov, D. M. Ho and G. C. Dismukes, *J. Am. Chem. Soc.*, 1994, **116**, 891-897.
3. Bruker, *APEX2 Ver. 2014.11-0, Bruker AXS Inc., Madison, WI, USA.*, 1-142.